Meta Learning of Interface Conditions for Multi-Domain Physics-Informed Neural Networks

Shibo Li[*]   SHIBO@CS.UTAH.EDU
School of Computing
University of Utah

Michael Penwarden[*]   MPENWARDEN@SCI.UTAH.EDU
Scientific Computing and Imaging Institute
University of Utah

Robert M. Kirby   KIRBY@CS.UTAH.EDU
School of Computing, Scientific Computing and Imaging Institute
University of Utah

Shandian Zhe   ZHE@CS.UTAH.EDU
School of Computing
University of Utah

Abstract

Physics-informed neural networks (PINNs) are emerging as popular mesh-free solvers for partial differential equations (PDEs). Recent extensions decompose the domain, applying different PINNs to solve the equation in each subdomain and aligning the solution at the interface of the subdomains. Hence, they can further alleviate the problem complexity, reduce the computational cost, and allow parallelization. However, the performance of the multi-domain PINNs is sensitive to the choice of the interface conditions for solution alignment. While quite a few conditions have been proposed, there is no suggestion about how to select the conditions according to specific problems. To address this gap, we propose META Learning of Interface Conditions (METALIC), a simple, efficient yet powerful approach to dynamically determine the optimal interface conditions for solving a family of parametric PDEs. Specifically, we develop two contextual multi-arm bandit models. The first one applies to the entire training procedure, and online updates a Gaussian process (GP) reward surrogate that given the PDE parameters and interface conditions predicts the solution error. The second one partitions the training into two stages, one is the stochastic phase and the other deterministic phase; we update a GP surrogate for each phase to enable different condition selections at the two stages so as to further bolster the flexibility and performance. We have shown the advantage of METALIC on four bench-mark PDE families.

1. Introduction

Physics-informed neural networks (PINNs) (Raissi et al., 2019a) are emerging as a popular mesh-free approach for solving partial differential equations (PDEs). They have shown success in many scientific and engineering problems, such as in bio-engineering (Sahli Costabal et al., 2020; Kissas et al., 2020), fluids mechanics (Raissi et al., 2019b; Sun et al., 2020; Raissi et al., 2020), and

---

. [*] Equal Contribution.

1

material design (Fang and Zhan, 2019; Liu and Wang, 2019). The recent multi-domain extensions, *e.g.*, (Jagtap et al., 2020; Jagtap and Karniadakis, 2021), further extend PINNs with a divide-and-conquer strategy, and have attracted considerable attention. Specifically, they decompose the domain of interest into several subdomains, place a separate PINN to solve the PDE at each subdomain, and then align the solutions at the interface of the subdomains. In this way, the multi-domain PINNs can alleviate problem complexity, adopt simpler architectures, reduce the training cost, and enable parallel computation (Shukla et al., 2021).

However, the performance of multi-domain PINNs is sensitive to the choice of interface conditions (or regularizers) that align the PINN solutions at different subdomains. Quite a few interface conditions have been proposed, such as those that encourage solution and residual continuity (Jagtap and Karniadakis, 2021), flux conservation (Jagtap et al., 2020), gradient continuity (De Ryck et al., 2022) and residual gradient continuity (Yu et al., 2022). On one hand, naively combining all possible interface conditions does not necessarily give the optimal performance; instead, it can complicate the loss landscape (Krishnapriyan et al., 2021), making the optimization more costly and challenging. On the other hand, the best interface conditions can vary across problems, which are up to the problem properties. Currently, there are no suggestions about how to select interface conditions according to specific problems, bringing inconvenience and difficulties to the multi-domain practice.

To address this issue, in this paper we propose METALIC, a simple, efficient and powerful meta learning method that can dynamically determine the best interface conditions for solving a family of parametric PDEs. Specifically, we develop two contextual multi-arm bandit (MAB) models. We view the PDE parameters as the context, sets of interface conditions as the arms, and the solution accuracy as the reward. Our first model applies to the whole training procedure, and online estimates a Gaussian process (GP) reward surrogate that predicts the solution accuracy given the context and binary encoding of the arm. We use Upper Confidence Bound (UCB) and Thompson sampling (TS) to fulfill effective exploration and exploitation tradeoffs. Due to the online nature of MAB, we can use the GP surrogate to select the optimal interface conditions given new PDE parameters while continuously improving the surrogate. Our second model partitions the training into two phases, the stochastic (*e.g.*, ADAM) and deterministic (*e.g.*, L-BFGS) phase. These two phases are often sequentially combined in PINNs to achieve reliable performance. We learn a separate contextual bandit, namely, a GP reward surrogate for each phase. In this way, we can select the optimal interface conditions for different training stages to enhance flexibility and to further improve performance. To coordinate the two bandits to optimize the final accuracy, we append the loss after the first phase into the context of the second bandit to predict the best conditions for training continuation; we add a discounted reward of the second bandit to the first one so as to integrate the influence of the first bandit on the subsequent training into its reward model updates.

We examined METALIC in four equation families: the Poisson, advection, reaction and Burger's equations, with parameters in the equation or boundary conditions. The evaluation of the online performance shows that the accumulated solution error of METALIC grows sublinearly, which is much slower than randomly selecting the arm at each play. The latter exhibits a linear growth. The results demonstrate that with more plays, our method keeps improving the reward surrogate while utilizing it to achieve promising solution accuracy. We then conducted a static test on a set of new PDEs after the online playing. With the interface conditions determined by our learned surrogate, the multi-domain PINNs achieve solution errors one order of magnitude smaller than using randomly selected conditions, which also outperform the standard single-domain PINNs.

2. Background

Physics-Informed Neural Networks (PINNs) estimate PDE solutions with (deep) neural networks, in light of the their universal approximation ability. Consider a PDE of the following general form,

$$\mathcal{F}[u](\mathbf{x}) = f(\mathbf{x}), \quad \mathbf{x} \in \Omega,$$
$$u(\mathbf{x}) = g(\mathbf{x}), \quad \mathbf{x} \in \partial\Omega \tag{1}$$

where $\mathcal{F}$ is the differential operator for the PDE, Ω is the domain, $\partial\Omega$ is the boundary of the domain, $f : \Omega \to \mathbb{R}$, and $g : \partial\Omega \to \mathbb{R}$ are the given source and boundary functions, respectively. To solve the PDE, the PINN uses a deep neural network $\widehat{u}_{\boldsymbol{\theta}}(\mathbf{x})$ to represent the solution u, samples N collocation points $\{\mathbf{x}_c^i\}_{i=1}^N$ from Ω and M points $\{\mathbf{x}_b^i\}_{i=1}^M$ from $\partial\Omega$, and minimizes the loss,

$$\boldsymbol{\theta}^* = \operatorname{argmin}_{\boldsymbol{\theta}} \ \lambda_b L_b(\boldsymbol{\theta}) + L_r(\boldsymbol{\theta}) \tag{2}$$

where $L_b(\boldsymbol{\theta}) = \frac{1}{M} \sum_{i=1}^M \left(\widehat{u}_{\boldsymbol{\theta}}(\mathbf{x}_b^i) - g(\mathbf{x}_b^i) \right)^2$ is the boundary term to fit the boundary condition, $L_r(\boldsymbol{\theta}) = \frac{1}{N} \sum_{i=1}^N \left(\mathcal{F}[\widehat{u}_{\boldsymbol{\theta}}](\mathbf{x}_c^i) - f(\mathbf{x}_c^i) \right)^2$ is the residual term to fit the equation, and $\lambda_b > 0$ is the weight of the boundary term. One can also add an initial condition term in the loss function to fit the initial conditions (when needed).

Multi-Domain PINNs decompose the domain Ω into several subdomains $\Omega_1, \ldots, \Omega_K$, and assign a separate PINN $\widehat{u}_{\boldsymbol{\theta}_k}$ to solve the PDE in each subdomain Ω_k. The loss for each PINN includes a boundary term $L_b^k(\boldsymbol{\theta}_k)$ and residual term $L_r^k(\boldsymbol{\theta}_k)$ similar to those in (2), based on the boundary and collocation points sampled from $\partial\Omega_k$ and Ω_k, respectively. In addition, to stitch the subdomains to obtain an overall solution over Ω, we introduce interface conditions into the loss to align the solutions of different PINNs at the intersection of the subdomains. There have been quite a few interface conditions. Suppose $\Omega_k \cap \Omega_{k'} \neq \emptyset$. We sample a set of interface points $\{\mathbf{x}_{k,k'}^i\}_{i=1}^{J_{k,k'}} \in \Omega_k \cap \Omega_{k'}$. One commonly used interface condition is to encourage the solution continuity (Jagtap and Karniadakis, 2021),

$$I_1(\boldsymbol{\theta}_k, \boldsymbol{\theta}_{k'}) = \frac{1}{J_{k,k'}} \sum_{i=1}^{J_{k,k'}} \left(\widehat{u}_{\boldsymbol{\theta}_k}(\mathbf{x}_{k,k'}^i) - \widehat{u}_{k,k'}^{\text{avg}}(\mathbf{x}_{k,k'}^i) \right)^2$$

where $\widehat{u}_{k,k'}^{\text{avg}}(\mathbf{x}_{k,k'}^i) = \frac{1}{2} \left(\widehat{u}_{\boldsymbol{\theta}_k}(\mathbf{x}_{k,k'}^i) + \widehat{u}_{\boldsymbol{\theta}_{k'}}(\mathbf{x}_{k,k'}^i) \right)$. A second one is the residual continuity (Jagtap and Karniadakis, 2021),

$$I_2(\boldsymbol{\theta}_k, \boldsymbol{\theta}_{k'}) = \frac{1}{J_{k,k'}} \sum_{i=1}^{J_{k,k'}} \left(\left(\mathcal{F}[\widehat{u}_{\boldsymbol{\theta}_k}](\mathbf{x}_{k,k'}^i) - f(\mathbf{x}_{k,k'}^i) \right) \right.$$
$$\left. - \left(\mathcal{F}[\widehat{u}_{\boldsymbol{\theta}_{k'}}](\mathbf{x}_{k,k'}^i) - f(\mathbf{x}_{k,k'}^i) \right) \right)^2. \tag{3}$$

Other choices include the gradient continuity (De Ryck et al., 2022) that encourages $\partial\widehat{u}_{\boldsymbol{\theta}_k}(\mathbf{x}_{k,k'}^i)/\partial\mathbf{x}_{k,k'}^i$ and $\partial\widehat{u}_{\boldsymbol{\theta}_{k'}}(\mathbf{x}_{k,k'}^i)/\partial\mathbf{x}_{k,k'}^i$ to be identical, the residual gradient continuity (Yu et al., 2022), flux conservation (Jagtap et al., 2020), *etc*. In general, the loss for each subdomain k has the following form

$$\mathcal{L}^k = \lambda_b L_b^k(\boldsymbol{\theta}_k) + L_r^k(\boldsymbol{\theta}_k) + \lambda_I \sum_{k':\Omega_{k'} \cap \Omega_k \neq \emptyset} \sum_{n \in \mathcal{S}} I_n(\boldsymbol{\theta}_k, \boldsymbol{\theta}_{k'})$$

where $\mathcal{S}$ is the set of interface conditions, and $\lambda_I > 0$ is the weight of the interface term. The training is to minimize $\mathcal{L} = \sum_{k=1}^{K} \mathcal{L}^k$. The final solution inside each sub-domain k is given by the associated PINN $\widehat{u}_{\boldsymbol{\theta}_k}$, while on the interface, by the average of the PINNs that share the interface.

3. Meta Learning of Interface Conditions

While multi-domain PINNs have shown successes, the selection of the interface conditions remains an open and difficult problem. On one hand, naively adding all possible conditions together will complicate the loss landscape, making the optimization challenging and expensive, yet not necessarily giving the best performance. On the other hand, different problems can demand a different set of the interface conditions as the best choice, which is up to the properties of the problem itself. Currently, there is a lack of methodologies to identify conditions for different problems. To address this issue, we propose METALIC, a meta learning approach to select problem-specific interface conditions. Specifically, we consider a parametric PDE family $\mathcal{A}$, where each PDE $\zeta \in \mathcal{A}$ is parameterized by $\boldsymbol{\beta} \in \mathcal{X} \subset \mathbb{R}^d$. The parameters can come from the operator $\mathcal{F}$, the source term f and/or the boundary function g (see (1)). Denote by $\mathcal{S} = \{I_1, \ldots, I_q\}$ the full set of interface conditions. Our goal is, given a PDE parameterized by arbitrary $\boldsymbol{\beta} \in \mathcal{X}$, to determine $I(\boldsymbol{\beta}) \subseteq \mathcal{S}$ — the best set of interface conditions — for multi-domain PINNs to solve that PDE.

3.1 Multi-Arm Bandit for Entire Training

We first propose a multi-arm bandit (MAB) model (Slivkins et al., 2019) to select the interface conditions for the entire training procedure of multi-domain PINNs. The MAB is a classical reinforcement learning problem. Consider a gambler playing q slot machines (*i.e.*, arms). Pulling the lever of each machine will return a random reward from a machine-specific probabilistic distribution, which is unknown apriori. The gambler aims to maximize the total reward earned from a series of lever-pulls across the q machines. For each play, the gambler needs to decide the tradeoff between exploiting the machine that has observed the largest expected payoff so far and exploring the payoffs of other machines. To determine PDE-specific interface conditions, we build a contextual MAB model. We consider the PDE parameters $\boldsymbol{\beta} \in \mathcal{X}$ as the state (context) of the system, all possible combinations of the interface conditions (*i.e.*, the power set of $\mathcal{S}$) as the arms, and the negative solution error as the reward. The problem space can be represented by a triplet $(\mathcal{X}, \mathcal{P}, r(\cdot, \cdot))$, where $\mathcal{X}$ is the state space, $\mathcal{P}$ is the action space (the power set of $\mathcal{S}$), and $r : \mathcal{X} \times \mathcal{P} \to \mathbb{R}$ is the reward function. We represent each action by a q-dimensional binary vector $\mathbf{a}$, where each element corresponds to a particular interface condition in $\mathcal{S}$. The i-th element $a_i = 1$ means the interface condition i is selected in the action.

To estimate the unknown reward function $r(\cdot, \cdot)$, we assign a Gaussian process (GP) prior,

$$r \sim \mathcal{GP}\left(0, \kappa\left([\boldsymbol{\beta}, \mathbf{a}], [\boldsymbol{\beta}', \mathbf{a}']\right)\right) \tag{4}$$

where $\kappa(\cdot, \cdot)$ is a kernel (covariance) function. Considering the categorical nature of the action input, we design a product kernel,

$$\kappa\left([\boldsymbol{\beta}, \mathbf{a}], [\boldsymbol{\beta}', \mathbf{a}']\right) = \kappa_1(\boldsymbol{\beta}, \boldsymbol{\beta}')\kappa_2(\mathbf{a}, \mathbf{a}') \tag{5}$$

4

where $\kappa_1(\boldsymbol{\beta}, \boldsymbol{\beta}') = \exp(-\tau_1 \|\boldsymbol{\beta} - \boldsymbol{\beta}'\|^2)$ is the square exponential (SE) kernel for continuous PDE parameters, and

$$\kappa_2(\mathbf{a}, \mathbf{a}') = \exp\left(\tau_2 \cdot \frac{1}{q} \sum_{i=1}^{q} \mathbb{1}(a_i = a_i')\right) \tag{6}$$

where $\mathbb{1}(\cdot)$ is the indicator function. Hence, the similarity between actions is based on the overlap ratio of the selected interface conditions, which is natural and intuitive.

To learn the MAB, each step we randomly sample a state $\boldsymbol{\beta}$ from $\mathcal{X}$, and then select an action $\mathbf{a}$, *i.e.*, a set of interface conditions, according to the current GP reward surrogate model. We then run the multi-domain PINNs with the interface conditions to solve the PDE parameterized by $\boldsymbol{\beta}$. We evaluate the negative solution error s as the received reward. We add the new data point $([\boldsymbol{\beta}, \mathbf{a}], -s)$ into the current training set, and retrain (update) the GP reward model. We repeat this procedure until a given maximum number of trials (plays) is finished. To fulfill a good exploration-exploitation tradeoff, we use the Upper Confidence Bound (UCB) (Auer, 2002; Srinivas et al., 2010) or Thompson sampling (TS) (Thompson, 1933; Chapelle and Li, 2011) to select the action at each step. Specifically, denote the current predictive distribution of the GP surrogate by

$$p(\widehat{r}|\mathcal{D}, \boldsymbol{\beta}, \mathbf{a}) = \mathcal{N}\left(\widehat{r}|\mu(\mathbf{a}, \boldsymbol{\beta}), \sigma^2(\mathbf{a}, \boldsymbol{\beta})\right)$$

where $\mathcal{D}$ is the accumulated training set so far. The UCB score is

$$\text{UCB}(\mathbf{a}) = \mu(\mathbf{a}, \boldsymbol{\beta}) + c \cdot \sigma(\mathbf{a}, \boldsymbol{\beta})$$

where $c > 0$, and the TS score is sampled from the predictive distribution,

$$\text{TS}(\mathbf{a}) \sim p(\widehat{r}|\mathcal{D}, \boldsymbol{\beta}, \mathbf{a}).$$

We can see that both scores integrate the predictive mean (which reflects the exploitation part) and the variance information (exploration part). We evaluate the score for each action $\mathbf{a} \in \mathcal{P}$ (UCB or TS), and then select the one with the highest score (corresponding to the best tradeoff).

In the online scenario, we can keep using UCB or TS to select the action for incoming new PDEs while improving the reward surrogate model according to the solution error. When the online playing is done and we no longer conduct exploration to update our model, given a new PDE (say, indexed by $\boldsymbol{\beta}^*$), we evaluate the predictive mean μ given $\boldsymbol{\beta}^*$ and every $\mathbf{a} \in \mathcal{P}$. We then select the one with the largest predictive mean (reward). We use the corresponding interface conditions to run the multi-domain PINNs to solve the PDE. Our MAB learning is summarized in Algorithm 1.

3.2 Sequential Multi-Arm Bandits

In practice, to achieve good and reliable performance, the training of PINNs is often divided into two stages. The first phase is stochastic training, typically with ADAM optimizer (Kingma and Ba, 2014), to find a nice valley of the loss landscape. The second phase is deterministic optimization, typically with L-BFGS, to ensure convergence to the (local) minimum. Due to the different nature of the two phases, the best interface conditions can vary as well. To enable more flexible choices so as to further improve the performance, we propose a sequential MAB model, as illustrated in Fig. 1. Specifically, for each training phase, we introduce a MAB similar to Sec 3.1, which updates a
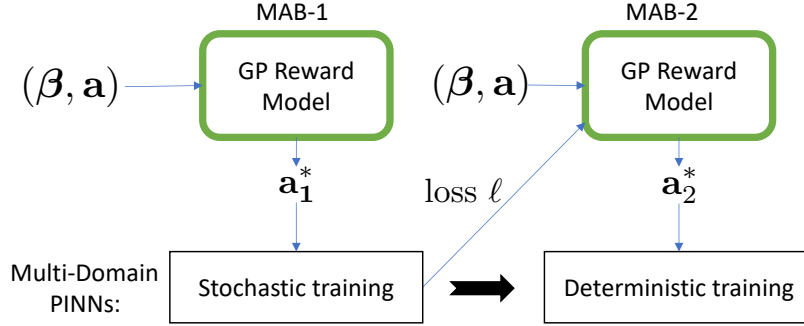
Figure 1: The illustration of the sequential MAB model.

separate GP reward model. To coordinate the two MABs to optimize the final accuracy, the reward of the first MAB, denoted by r_1, includes not only the negative solution error after the stochastic training phase, but also a discounted error after the second phase,

$$r_1 = -s_1 + \gamma \cdot (-s_2) \tag{7}$$

where γ is the discount factor, and s_1 and s_2 are the solution errors after the stochastic and deterministic training phases, respectively. In this way, the influence of the interface conditions at the first training phase on the final solution accuracy is also integrated into the learning of the GP reward model. Next, we expand the context of the second MAB with the training loss after the first phase. The system state includes both the PDE parameters β and the loss value ℓ, which together with the action $\mathbf{a}$ constitute the input to the GP reward model of the second MAB. In this way, the training status of the first phase is also used to determine the interface conditions for the second phase.

To learn our sequential MAB model, each step we randomly sample the PDE parameters $\beta \in \mathcal{X}$. Then based on the GP reward model of the first MAB, we use UCB (or TS) to select an action (*i.e.*, the first set of interface conditions), with which we conduct the stochastic training of the multi-domain PINNs. We then feed the training loss ℓ, PDE parameters β and every possible action into the GP reward model of the second MAB. We select the second set of interface conditions, with which to continue the training of the multi-domain PINNs using deterministic optimization. We evaluate the solution error after each phase, and obtain the reward and new examples for the two GP reward models. We update these models accordingly. The learning of the sequential MABs is summarized in Algorithm 2.

4. Related Work

As an alternative to mesh-based numerical methods, PINNs have achieved many success stories, *e.g.*, (Raissi et al., 2020; Chen et al., 2020; Sirignano and Spiliopoulos, 2018; Zhu et al., 2019; Geneva and Zabaras, 2020; Sahli Costabal et al., 2020). Multi-domain PINNs, *e.g.*, XPINNs (Jagtap and Karniadakis, 2021) and cPINNs (Jagtap et al., 2020), extend PINNs based on domain decomposition and use a set of PINNs to solve the PDE in different subdomains. To align the solutions across the subdomains, XPINNs used solution continuity and residual continuity as the interface conditions. Other conditions are also available, such as the flux conservation in cPINNs (Jagtap et al., 2020), the gradient continuity (De Ryck et al., 2022), and the residual gradient continuity in gPINNs (Yu et al.,

---

Algorithm 1 METALIC-single(T)

1: Initialize the GP reward surrogate model, and $\mathcal{D} \leftarrow \emptyset$.
2: **repeat**
3:      Randomly sample the PDE parameters $\boldsymbol{\beta} \in \mathcal{X}$
4:      For each action $\mathbf{a} \in \mathcal{P}$, compute the predictive distribution of the GP reward model, $\mathcal{N}\left(\mu(\mathbf{a}, \boldsymbol{\beta}), \sigma^2(\mathbf{a}, \boldsymbol{\beta})\right)$
5:      Compute the UCB score: $\text{UCB}(\mathbf{a}) = \mu + c \cdot \sigma$ or TS score: $\text{TS}(\mathbf{a}) \sim \mathcal{N}(\mu, \sigma^2)$
6:      $\mathbf{a}^* = \text{argmax}_{\mathbf{a} \in \mathcal{P}} \text{UCB}(\mathbf{a})$ or $\mathbf{a}^* = \text{argmax}_{\mathbf{a} \in \mathcal{P}} \text{TS}(\mathbf{a})$
7:      Use the interface conditions of $\mathbf{a}^*$ to train the multi-domain PINNs to solve the PDE parameterized by $\boldsymbol{\beta}$, and evaluate the solution error s
8:      $\mathcal{D} \leftarrow \mathcal{D} \cup \{([\mathbf{a}^*, \boldsymbol{\beta}], -s)\}$
9:      Retrain the GP reward model on $\mathcal{D}$
10: **until** T iterations are done

Algorithm 2 METALIC-seq(γ, T)

1: Initialize two GP reward models. Set their training sets $\mathcal{D}_1$ and $\mathcal{D}_2$ to empty.
2: **repeat**
3:      Randomly sample $\boldsymbol{\beta} \in \mathcal{X}$
4:      Based on the predictive distribution of the first GP model, use UCB or TS to select the best action $\mathbf{a}_1^*$.
5:      Use the interface conditions of $\mathbf{a}_1^*$ to train the multi-domain PINNs with ADAM. Evaluate the error s_1 for solving the PDE parameterized by $\boldsymbol{\beta}$.
6:      Given the current training loss ℓ and $\boldsymbol{\beta}$, compute the predictive distribution of the second GP reward model for each action, and use UCB or TS to select the best action $\mathbf{a}_2^*$.
7:      Use the interface conditions of $\mathbf{a}_2^*$ to continue the training with L-BFGS. Evaluate the solution error s_2.

8:      $\mathcal{D}_1 \leftarrow \mathcal{D}_1 \cup \{([\mathbf{a}^*, \boldsymbol{\beta}], -s_1 - \gamma s_2)\}, \mathcal{D}_2 \leftarrow \mathcal{D}_2 \cup \{([\mathbf{a}^*, \boldsymbol{\beta}, \ell], -s_2)\}$
9:      Retrain the two GP models on $\mathcal{D}_1$ and $\mathcal{D}_2$, respectively.
10: **until** T iterations are done

2022). Recently, Hu et al. (2021) developed a theoretical understanding on the convergence and generalization properties of XPINNs, and empirically examined when XPINNs outperform PINNs.

Meta-learning (Schmidhuber, 1987; Naik and Mammone, 1992; Thrun and Pratt, 2012) is an important topic in machine learning. The existing works can be roughly attributed to three categories: (1) metric-learning that learns a metric space with which the tasks can make predictions via matching the training points, *e.g.*, nonparametric nearest neighbors (Koch et al., 2015; Vinyals et al., 2016; Snell et al., 2017; Oreshkin et al., 2018; Allen et al., 2019), (2) learning black-box models (*e.g.*, neural networks) that map the task dataset and hyperparameters to the optimal model parameters or parameter updating rules, *e.g.*, (Hochreiter et al., 2001; Andrychowicz et al., 2016; Li and Malik, 2016; Ravi and Larochelle, 2017; Santoro et al., 2016; Duan et al., 2016; Wang et al., 2016; Munkhdalai and Yu, 2017; Mishra et al., 2017), and (3) bi-level optimization where the outer level optimizes the hyperparameters and the inner level optimizes the model parameters given the hyperparameters (Finn et al., 2017; Finn, 2018; Bertinetto et al., 2018; Lee et al., 2019; Zintgraf et al., 2019; Li et al., 2017; Finn et al., 2018; Zhou et al., 2018; Harrison et al., 2018). A recent influential work is the model-agnostic meta learning (MAML) (Finn et al., 2017), which uses the bi-level optimization framework to learn a good model initialization for a family of tasks. There have been a large number of subsequent works, such as (Grant et al., 2018; Yoon et al., 2018; Finn et al., 2018; Song et al., 2020; Liu et al., 2019; Penwarden et al., 2021). In our work, the task family consists

of parametric PDEs, and the learning model is the multi-domain PINNs. The hyperparameters are the set of interface conditions, not the model initialization. Another difference is that our method predicts task-specific hyperparameters, rather than assumes one single set of conditions apply to all the tasks (PDEs).

Multi-arm bandit is a classical online decision making framework (Lai et al., 1985; Auer et al., 2002a,b; Mahajan and Teneketzis, 2008; Bubeck et al., 2012), and have numerous applications, such as online advertising (Avadhanula et al., 2021), collaborative filtering (Li et al., 2016), clinical trials (Aziz et al., 2021) and robot control (Laskey et al., 2015). To our knowledge, our work is the first to use MAB for meta learning of task-specific hyperparameters , which is advantageous in its simplicity and efficiency. MAB can be viewed as an instance of reinforcement learning (RL) (Sutton and Barto, 2018). But it only needs to online estimates a reward function. While one can design more expressive RL models to meanwhile learn a Markov decision process (in MAB, we simply use UCB or TS), it often demands we run a massive number of PINN training trajectories, which is much more expensive. The model estimation is also much more challenging.

5. Experiment

To evaluate METALIC, we considered four benchmark equation families. We list the equations and domain decomposition settings in the following.

The Poisson Equation. First, we considered a 2D Poisson equation with a parameterized source function,

$$u_{xx} + u_{yy} = \widetilde{f}(x, y; s) \tag{8}$$

where $(x, y) \in [0, 1] \times [0, 1]$, $\widetilde{f}(x, y; s) = f(x, y; s) / \max_{x,y} f(x, y; s)$, and

$$\begin{aligned}
f(x, y; s) = &[\text{erf}((x - 0.25)s) - \text{erf}((x - 0.75)s)] \\
&\cdot [\text{erf}((y - 0.25)s) - \text{erf}((y - 0.75)s)],
\end{aligned} \tag{9}$$

where $\text{erf}(z) = \frac{2}{\sqrt{\pi}} \int_0^z e^{-t^2} \mathrm{d}t$, and $s \in [0, 50]$ is called the sharpness parameter that controls the sharpness of the interior square in the source. We used Dirichlet boundary conditions, and ran a finite difference solver to obtain an accurate "gold-standard" solution. To run multi-domain PINNs, we split the domain into two subdomains, where the interface is a line at $y = 0.5$. We visualize an exemplar solution and the subdomains, including the sampled boundary and collocation points in Fig. 2.

Advection Equation. We next considered a 1D advection (one-way wave) equation,

$$u_t + \beta u_x = 0$$

where $x \in [0, 2\pi]$, $t \in [0, 1]$, and β is the PDE parameter denoting the wave speed. We used Dirichlet boundary conditions, and the solution has an analytical form, $u(x, t) = h(x - \beta t)$ were $h(x)$ is the initial condition (which we select as $h(x) = \sin(x)$). For domain decomposition, we split the domain at $t = 0.5$ to obtain two subdomains. Fig. 3 shows an exemplar solution and the subdomains with the interface.

Reaction Equation. Third, we evaluate a 1D reaction equation,

$$u_t - \rho u(1 - u) = 0$$

(a) Solution at $s = 20$
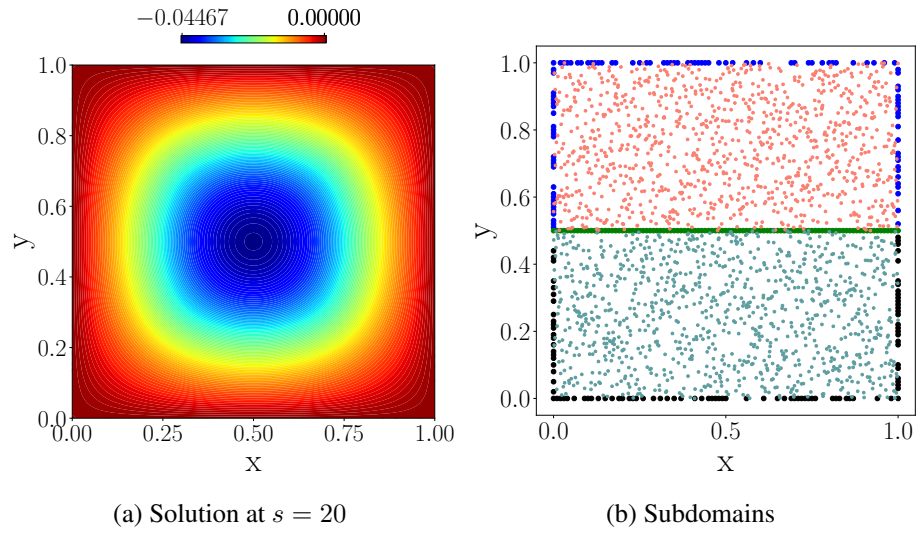
(b) Subdomains

Figure 2: The Poisson equation. The interface is the green line at $y = 0.5$. Blue and black dots show the sampled boundary points in each subdomain, and the internal dots (red and cyan) are the sampled collocation points inside each subdomain.


(a) Solution at $\beta = 30$

(b) Subdomains
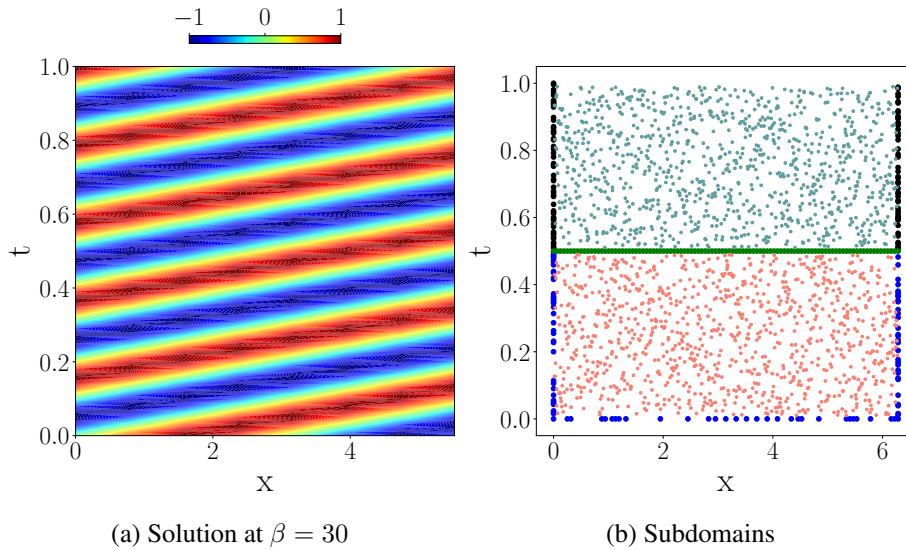
Figure 3: Advection equation. The interface is the green line at $t = 0.5$.

9

(a) Solution at $\rho = 5.0$ (b) Subdomains
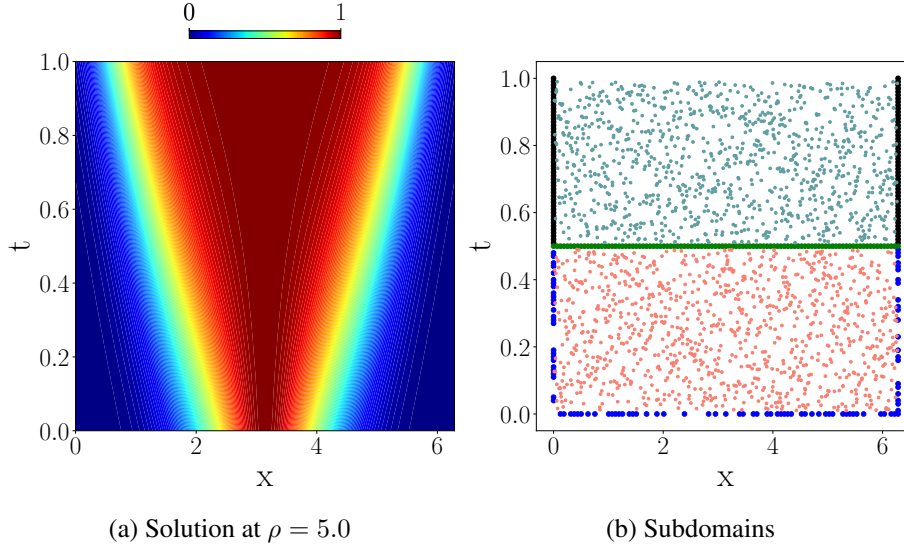
Figure 4: Reaction equation. The interface is at $t = 0.5$.

where ρ is the reaction coefficient (ODE parameter), $x \in [0, 2\pi]$, $t \in [0, 1]$ and $u(x, 0) = e^{-\frac{(x-\pi)^2}{2(\pi/4)^2}}$. The exact solution is $u(x, t) = u(x, 0) \cdot [e^{\rho t} / (u(x, 0)e^{\rho t} + 1 - u(x, 0))]$. We split the domain at $t = 0.5$ to obtain two subdomains. Although not required for well-posedness of the ODE system, because we are solving for the PINN space-time field $u(x, t)$, we use the exact solution to define a boundary loss term. This enhances training without compromising the time partitioning we wish to highlight. We show a solution example and the subdomains in Fig. 4.

Burger's Equation. Fourth, we considered the viscous Burger's equation,

$$u_t + uu_x = \nu u_{xx}$$

where $\nu \in [0.001, 0.05]$ is the viscosity (PDE parameter), $x \in [-1, 1]$, $t \in [0, 1]$, and $u(x, 0) = -\sin(\pi x)$. We ran a numerical solver to obtain an accurate "gold-standard" solution. To decompose the domain, we take the middle portion that includes the shock waves as one subdomain, namely, $\Omega_1 : x \in [-0.1, 0.1], t \in [0, 1]$, and the remaining as the other subdomain, $\Omega_2 : x \in [-1, -0.1] \cap [0.1, 1], t \in [0, 1]$. Hence, the interface consists of two lines. See Fig. 5 for the illustration and solution example.

To evaluate METALIC, we used 9 interface conditions, which are listed in the supplementary material. For the PINN in each subdomain, we used two layers, with 20 neurons per layer and tanh activation function. We randomly sampled 1,000 collocation points and 100 boundary points for each PINN. To inject the interface conditions, we then randomly sampled 101 interface points for the Poisson, advection and reaction equations, and 802 interface points for Burger's equation. We set $\lambda_b = 20$ and $\lambda_I = 5$, which follows the insight of (Wang et al., 2021, 2022) to adopt large weights for the boundary and interface terms so as to prevent the training of PINNs from being dominated by the residual term. We denote our single MAB by METALIC-single, and sequential MABs by METALIC-seq. For the latter, we set the discount factor $\gamma = 0.9$ (see (7)). For better numerical stability, we used the relative L_2 error in the log domain to obtain the reward for updating the GP surrogate models. The running of the multi-domain PINNs consists of 10K ADAM epochs (with

10

(a) Solution at $\nu = 0.001$
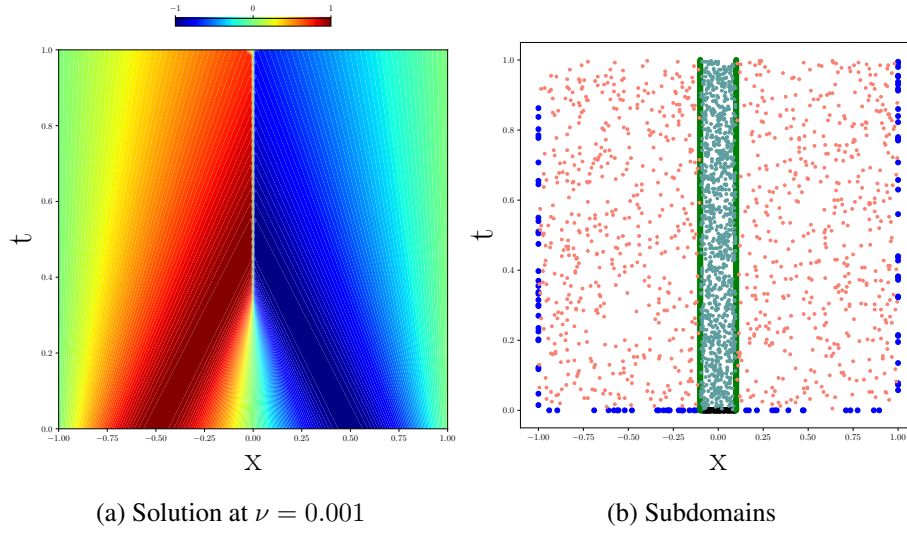
(b) Subdomains

Figure 5: Burger's equation. The interfaces are at $x = -0.1$ and $x = 0.1$. The middle portion (filled with cyan dots) is the first subdomain, and the remaining parts constitute the second subdomain.


(a) Poisson equation   (b) Advection equation   (c) Reaction equation   (d) Burgers' equation
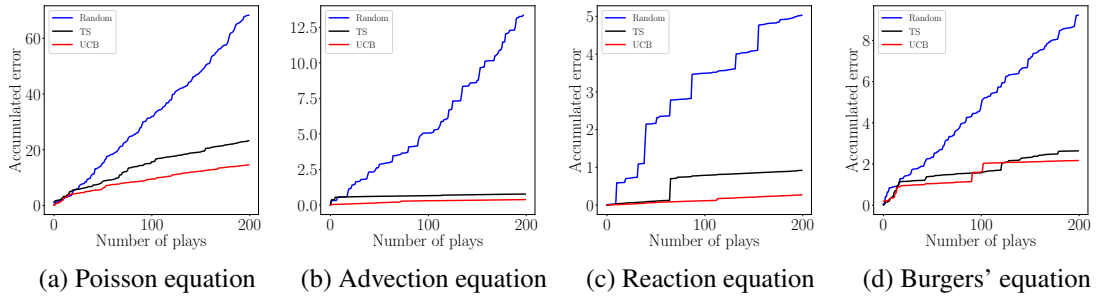
Figure 6: Online performance of METALIC-single.

(a) Poisson equation   (b) Advection equation   (c) Reaction equation   (d) Burgers' equation
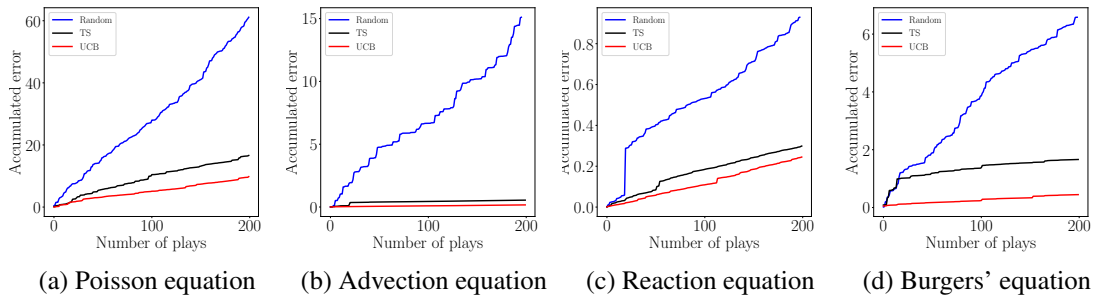
Figure 7: Online performance of METALIC-seq.
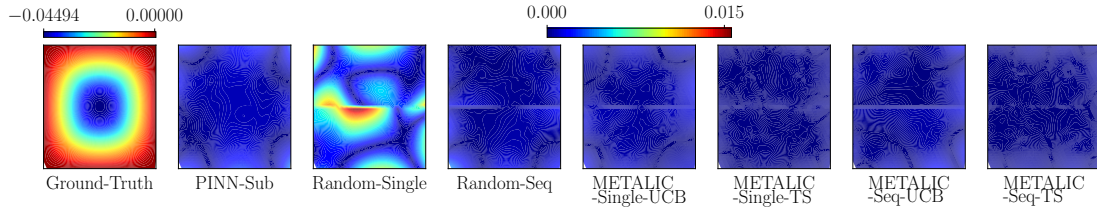
(a) Poisson equation ($s = 46.1$)
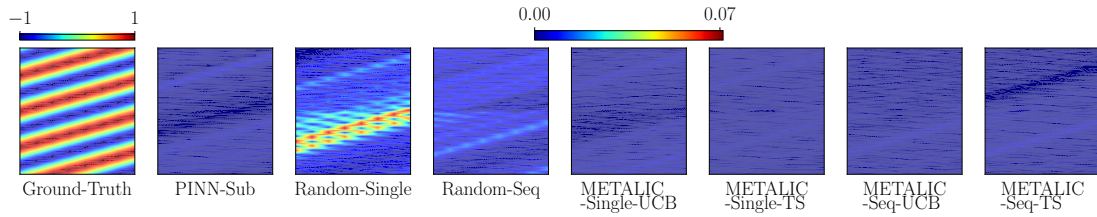
(b) Advection equation ($\beta = 24.02$)
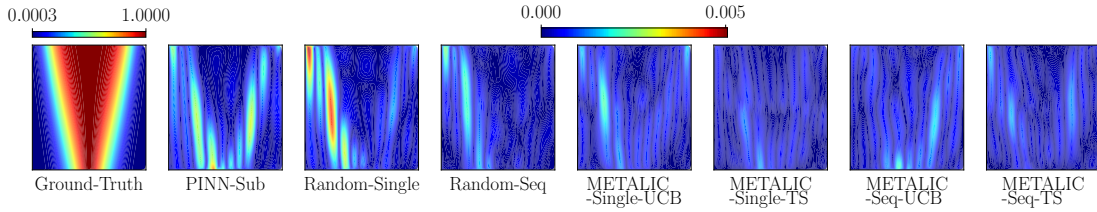
(c) Reaction equation ($\rho = 4.1$)
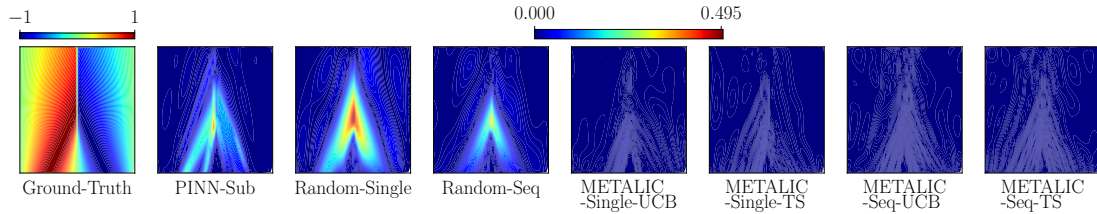
(d) Burgers' equation ($\nu = 0.0036$)

Figure 8: Point-wise solution error.

Method	Poisson	Advection	Reaction	Burger's
Random-Single	0.3992 ± 0.0037	0.07042 ± 0.01575	0.00612 ± 0.000278	0.04021 ± 0.00057
Random-Seq	0.3004 ± 0.0032	0.03922 ± 0.00919	0.01284 ± 0.000707	0.03486 ± 0.00066
PINN-Sub	0.03078 ± 0.00177	$0.00130 \pm 8.108\text{e-}5$	0.00213 ± 0.00021	0.00738 ± 0.00313
PINN-Merge-H	0.02398 ± 0.00144	$0.00098 \pm 5.038\text{e-}5$	0.00223 ± 0.00026	0.00951 ± 0.00390
PINN-Merge-V	0.02184 ± 0.00211	$0.00079 \pm 3.391\text{e-}5$	$\mathbf{0.00099 \pm 0.00013}$	0.00276 ± 0.00041
METALIC-Single-TS	0.02503 ± 0.0002	$0.00079 \pm 4.5897\text{e-}5$	$0.00204 \pm 1.013\text{e-}4$	$\mathbf{0.00109 \pm 1.306\text{e-}5}$
METALIC-Single-UCB	0.0245 ± 0.0002	$0.00078 \pm 3.6771\text{e-}5$	$0.00102 \pm 8.945\text{e-}6$	$0.00161 \pm 2.939\text{e-}5$
METALIC-Seq-TS	$0.01639 \pm 9.5384\text{e-}5$	$0.00078 \pm 3.6473\text{e-}5$	$\mathbf{0.00099 \pm 8.4704\text{e-}6}$	$0.00152 \pm 5.571\text{e-}5$
METALIC-Seq-UCB	$\mathbf{0.01406 \pm 9.1099\text{e-}5}$	$\mathbf{0.00070 \pm 3.2790\text{e-}5}$	$0.00099 \pm 5.999\text{e-}6$	$0.00139 \pm 3.948\text{e-}5$

Table 1: The average L_2 relative error of single-domain PINNs and multi-domain PINNs for solving 100 test PDEs. The interface conditions of the multi-domain PINNs are provided by METALIC and random selection. {Single, Seq} indicate using a single set or two sequential sets of interface conditions for the running of the multi-domain PINNs. {TS, UCB} corresponds to our method using TS or UCB score to determine the interface conditions at each play.

learning rate 10^{-3}) and then 50K L-BFGS iterations (the first order optimality and parameter change tolerances set to 10^{-6} and 10^{-9} respectively). We set $c = 1$ to compute the UCB score. We ran 200 plays (trials) for our method. For static (offline) test, we randomly sampled 100 PDEs (which do not overlap with the PDEs sampled during the online playing). We then used the learned reward model to determine the best interface conditions for each particular PDE (according to the predictive mean), with which we ran the multi-domain PINNs to solve the PDE, and computed the relative L_2 error.

First, to examine the online performance of METALIC, we looked into the accumulated solution error along with the number of plays. We compared with randomly selecting the arm at each play. In the case of running METALIC-seq, this baseline correspondingly randomly selects the arm twice, one at the stochastic training phase, and the other at the deterministic phase. The results are shown in Fig. 6 and 7. As we can see, the accumulated error of METALIC with both UCB and TS grows much slower, *i.e.*, sublinearly, than the random selection approach (note that the reward of the optimal action is unknown due to the randomness in the running of PINNs, and we cannot compute the regret). This has shown that our method achieves a much better exploration-exploitation tradeoff in the online interface condition decision and model updating, which is consist with many other MAB applications (see Sec 4). The results demonstrate the advantage of our MAB-based approach. First, via effective exploration, METALIC can collect valuable training examples (rewards at new actions and context) to improve the learning efficiency and performance of the GP reward surrogate model. Second, the online decision also takes advantage of the predictive abaility of the current reward model, *i.e.*, exploitation, to select effective interface conditions, which results in increasingly better solution accuracy of the multi-domain PINNs. The online nature of METALIC enables us to keep improving the reward model while utilizing it to solve new equations with promising accuracy.

Next, we conducted an offline test, namely, without online exploration and model updates any more after 200 plays. We compared with (1) Random-Single, which, for each PDE, randomly selects a set of interface conditions applied to the entire training of the multi-domain PINNs, and (2) Random-Seq, which for each PDE, randomly selects two sets of interface conditions, one for the stochastic training and the other for the deterministic training phase. We also tested single-domain PINNs that do not incorporate interface conditions. Specifically, we compared with (3) PINN-Sub, which used the same architecture as the PINN in each subdomain, but applied to the entire domain, (4) PINN-Merge-H, which horizontally pieced all the PINNs in the subdomains, *i.e.*, doubling the layer

width yet fixing the depth, (5) PINN-Merge-V, which vertically stacked the PINNs, *i.e.*, doubling the depth while fixing the width. Note that while PINN-Merge-H and PINN-Merge-V merge the PINNs in each subdomain, the total number of neurons actually increases (for connecting these PINNs). Hence, the merged PINN is more expressive. Each single-domain PINN used the union of the boundary points and collocation points from every subdomain. We used the same weight for the boundary term, *i.e.*, $\lambda_b = 20$. The running of each single-domain PINN follows exactly the same setting of the multi-domain PINNs (*i.e.*, 10K ADAM epochs and 50K L-BFGS iterations).

We report the average relative L_2 solution error and the standard deviation in Table 1. As we can see, randomly selecting interface conditions, no matter for the whole training procedure or two training phases, result in much worse solution accuracy of multi-domain PINNs. The solution error is one order of magnitude bigger than METALIC in all the settings. It confirms that the success of the multi-domain PINNs is up to appropriate interface conditions. Next, we can observe that while the performance of METALIC-Single is similar to METALIC-Seq, the best solution accuracy is in most cases obtained by interface conditions selected by METALIC-Seq (except in solving the Burger's equation). It demonstrates that our sequential MAB model that can employ different conditions for the two training phases is more flexible and brings additional improvement. We also observe that in most cases using the UCB for online playing can lead to better performance for both METALIC-Single and METALIC-Seq. This is consistent with the online performance evaluation (see Fig. 6 and 7). Third, among the single-domain PINN methods, PINN-Merge-V outperforms PINN-sub in all the equation families and PINN-Merge-H outperforms PINN-sub in the Poisson and advection equations, showing that deeper or wider architectures can help further improve the solution accuracy. However, their performance is still second to the best setting of METALIC, which uses simpler subdomain PINN architectures and fewer total learnable parameters. These multi-domain PINNs can be further parallelized to accelerate training. By contrast, if the interface conditions are inferior, such as those selected by Random-Single and Random-Seq, the solution error becomes much worse (orders of magnitude bigger) than single-domain PINNs. Together these results have shown the importance of the interface conditions for multi-domain PINNs and the advantage of our method.

For a fine-grained comparison, we visualize the point-wise solution error of PINN-Sub, Random-Single, Random-Seq, and our method in solving four random instances of the equations. As shown in Fig. 8, the point-wise error of both METALIC-Single and METALIC-Seq is quite uniform across the domain and close to zero (dark blue). By contrast, the competing methods often exhibit relative large errors in a few local regions, *e.g.*, those in the middle (where the shock waves appear) of the domain of the Burger's equation (PINN-Sub, Random-Single, Random-Seq), and the central part of the domain of the Poisson and advection equation (Random-Single). It shows that our method not only can give a superior global accuracy, but locally also better recovers individual solution values.

Finally, we analyzed the selected interface conditions in each equation family by METALIC. We found that those conditions are interesting, physically meaningful, and consistent with the properties of the equations. Due to the space limit, we provide the detailed analysis and discussion in the supplementary material.

6. Conclusion

We have presented METALIC, a simple, efficient and powerful meta learning approach to select PDE-specific interface conditions for general multi-domain PINNs. The results at four bench-mark

equation families are encouraging. In the future, we will extend our method to also meta learn the interface locations as well as the conditions, as a function of not only accuracy but training time so as to improve both the solution accuracy and training efficiency of the multi-domain PINNs.

Appendix A. Interface Conditions

We used a total number of 9 interface conditions throughout all the experiments, which are listed in Table 1. Note that I_z and I_{zz} correspond to the first and second-order derivatives w.r.t an input to the PDE solution function. Since all the test PDE problems consist of two spatial or spatiotemporal dimensions, I_z and I_{zz} give four interface conditions. There are no mixed derivatives across different input dimensions. In the case that one I_z is the same as I_c, such as in Poisson equation, the de-duplication gives 9 different conditions. In the case that all I_z's are different from I_c, such as in Burger's equation, we used I_c and removed one I_z ($z = y$ or $z = t$), so that we still maintain 9 interface conditions to be consistent with other experiments.

Table 2: Interface Conditions of Multi-domain PINNs

I_u	Solution continuity (10)
$I_{u_{avg}}$	Average solution continuity (11)
I_r	Residual (12)
I_{rc}	Residual continuity (13)
I_{gr}	Gradient-enhanced residual (14)
I_c	Flux continuity (15)
I_z	First-order spatial/temporal derivative continuity (16)
I_{zz}	Second-order spatial/temporal derivative continuity (17)

$$I_u(\boldsymbol{\theta}_k, \boldsymbol{\theta}_{k'}) = \frac{1}{J_{k,k'}} \sum_{i=1}^{J_{k,k'}} \left(\widehat{u}_{\boldsymbol{\theta}_k}(\mathbf{x}_{k,k'}^i) - \widehat{u}_{\boldsymbol{\theta}_{k'}}(\mathbf{x}_{k,k'}^i) \right)^2 \tag{10}$$

$$I_{u_{avg}}(\boldsymbol{\theta}_k, \boldsymbol{\theta}_{k'}) = \frac{1}{J_{k,k'}} \sum_{i=1}^{J_{k,k'}} \left(\widehat{u}_{\boldsymbol{\theta}_k}(\mathbf{x}_{k,k'}^i) - \widehat{u}_{k,k'}^{\text{avg}}(\mathbf{x}_{k,k'}^i) \right)^2 \tag{11}$$

$$\text{where } \widehat{u}_{k,k'}^{\text{avg}}(\mathbf{x}_{k,k'}^i) = \frac{1}{2} \left(\widehat{u}_{\boldsymbol{\theta}_k}(\mathbf{x}_{k,k'}^i) + \widehat{u}_{\boldsymbol{\theta}_{k'}}(\mathbf{x}_{k,k'}^i) \right)$$

$$I_r(\boldsymbol{\theta}_k, \boldsymbol{\theta}_{k'}) = \frac{1}{J_{k,k'}} \sum_{i=1}^{J_{k,k'}} \left(\left(\mathcal{F}[\widehat{u}_{\boldsymbol{\theta}_k}](\mathbf{x}_{k,k'}^i) - f(\mathbf{x}_{k,k'}^i) \right)^2 + \left(\mathcal{F}[\widehat{u}_{\boldsymbol{\theta}_{k'}}](\mathbf{x}_{k,k'}^i) - f(\mathbf{x}_{k,k'}^i) \right)^2 \right) \tag{12}$$

$$I_{rc}(\boldsymbol{\theta}_k, \boldsymbol{\theta}_{k'}) = \frac{1}{J_{k,k'}} \sum_{i=1}^{J_{k,k'}} \left(\left(\mathcal{F}[\widehat{u}_{\boldsymbol{\theta}_k}](\mathbf{x}_{k,k'}^i) - f(\mathbf{x}_{k,k'}^i) \right) - \left(\mathcal{F}[\widehat{u}_{\boldsymbol{\theta}_{k'}}](\mathbf{x}_{k,k'}^i) - f(\mathbf{x}_{k,k'}^i) \right) \right)^2 \tag{13}$$

$$I_{gr}(\boldsymbol{\theta}_k, \boldsymbol{\theta}_{k'})$$
$$= \frac{1}{J_{k,k'}} \sum_{i=1}^{J_{k,k'}} \sum_{j=1}^{2} \left(\left| \frac{\partial}{\partial \mathbf{x}_{k,k'}^i[j]} \left(\mathcal{F}[\widehat{u}_{\boldsymbol{\theta}_k}](\mathbf{x}_{k,k'}^i) - f(\mathbf{x}_{k,k'}^i) \right) \right|^2 + \left| \frac{\partial}{\partial \mathbf{x}_{k,k'}^i[j]} \left(\mathcal{F}[\widehat{u}_{\boldsymbol{\theta}_{k'}}](\mathbf{x}_{k,k'}^i) - f(\mathbf{x}_{k,k'}^i) \right) \right|^2 \right) \tag{14}$$

$$I_c(\boldsymbol{\theta}_k, \boldsymbol{\theta}_{k'}) = \frac{1}{J_{k,k'}} \sum_{i=1}^{J_{k,k'}} \left(\phi\left(\widehat{u}_{\boldsymbol{\theta}_k}(\mathbf{x}_{k,k'}^i)\right) \cdot \mathbf{n} - \phi\left(\widehat{u}_{\boldsymbol{\theta}_{k'}}(\mathbf{x}_{k,k'}^i)\right) \cdot \mathbf{n} \right)^2 \tag{15}$$

where $\phi(\widehat{u}_{\boldsymbol{\theta}}) \cdot \mathbf{n}$ are fluxes normal at the interface

$$I_z(\boldsymbol{\theta}_k, \boldsymbol{\theta}_{k'}) = \frac{1}{J_{k,k'}} \sum_{i=1}^{J_{k,k'}} \left(\frac{\partial}{\partial z^i} \widehat{u}_{\boldsymbol{\theta}_k}(\mathbf{x}_{k,k'}^i) - \frac{\partial}{\partial z^i} \widehat{u}_{\boldsymbol{\theta}_{k'}}(\mathbf{x}_{k,k'}^i) \right)^2 \tag{16}$$

where $z^i = \mathbf{x}_{k,k'}^i[1]$ or $z^i = \mathbf{x}_{k,k'}^i[2]$.

$$I_{zz}(\boldsymbol{\theta}_k, \boldsymbol{\theta}_{k'}) = \frac{1}{J_{k,k'}} \sum_{i=1}^{J_{k,k'}} \left(\frac{\partial^2}{\partial z^{i^2}} \widehat{u}_{\boldsymbol{\theta}_k}(\mathbf{x}_{k,k'}^i) - \frac{\partial^2}{\partial z^{i^2}} \widehat{u}_{\boldsymbol{\theta}_{k'}}(\mathbf{x}_{k,k'}^i) \right)^2 \tag{17}$$

where $z^i = \mathbf{x}_{k,k'}^i[1]$ or $z^i = \mathbf{x}_{k,k'}^i[2]$.

Appendix B. Preliminary Study of the Interface Conditions

We conducted a preliminary study on a 2D Poisson equation $u_{xx} + u_{yy} = 1$ with the solution shown in Figure 9.
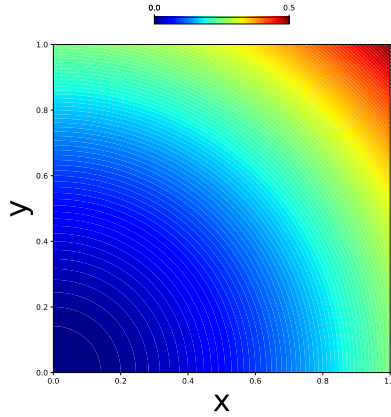

Figure 9: Poisson solution.

Given this PDE problem, we compared three types of boundary and collocation point sampling methods: random, grid, and Poisson disc sampling, as shown in Figure 10. The comparison was done between a standard PINN and XPINN, where the number of collocation points in each XPINN subdomain is the same as the total number of collocation points used by the PINN. We trained the two models with the boundary loss term weight λ_b set to 1 and 20. We also varied the interface loss term weight λ_I from $\{1, 20\}$. The interface loss term is computed from (11) and (13). Table 3 shows the L_2 relative error averaged over 10 runs to minimize the variance in network initialization

17

and optimization. We can see that the XPINN performance is relevantly less variant to differences in sampling and weights, but for PINNs these differences result in order of magnitude changes in error. For this reason, we have conducted all the evaluations fairly by using random sampling and larger boundary weights for PINN's which was the best overall setting. We also make the insight that random sampling allows a PINN to see higher frequencies according to the Nyquist-Shannon sampling theorem which may be the reason for increased performance over the other sampling methods. But the XPINN has the additional complexity of subdomains and interface conditions which may dominate the training resulting and give less varying performance across all the sampling methods.

(a) Random (b) Grid (c) Poisson Disc
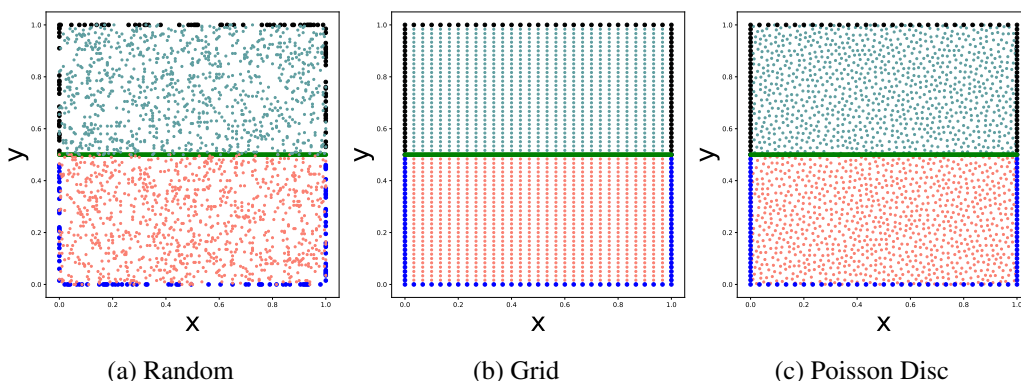
Figure 10: Random, grid, and Poisson disc sampling for the Poisson equation problem. The interface is the green line at $y = 0.5$. Blue and black dots show the sampled boundary points in each subdomain, and the internal dots (red and cyan) the sampled points inside each subdomain.

Model	Random		Grid		Poisson Disc	
	$\lambda_{b,I} = 1$	$\lambda_{b,I} = 20$	$\lambda_{b,I} = 1$	$\lambda_{b,I} = 20$	$\lambda_{b,I} = 1$	$\lambda_{b,I} = 20$
PINN	9.0325e-4	**4.3223e-4**	6.0278e-3	2.3699e-3	5.3902e-3	2.2375e-3
XPINN	5.0884e-3	5.3205e-3	6.0764e-3	4.7829e-3	6.5061e-3	4.4888e-3

Table 3: Average L_2 relative error over 10 runs for different sampling techniques and loss term weights.

B.1 Interface Condition Combination

For the same PDE problem with random sampling, we ran multi-domain PINNs with different sets of conditions. We used the generalized interface condition notations for multi-domain PINNs as described in Table 2. For example, an XPINN can be described as $I_{u_{avg}} + I_{rc}$. The weights on all terms are unity. As seen by the results in Table 4, the multi-domain PINNs with interfaces $I_{u_{avg}} + I_c + I_{yy}$ outperforms the rest as well as the PINN. We can see that with the correct interface conditions, the multi-domain PINN can greatly improve upon the standard XPINN. In fact, the additional residual continuity term, a trait of XPINNs, performs infinitesimally better than only using the average solution continuity. These results are the foundation of the METALIC method as we have shown that different combinations of conditions result in drastically different performances. We can also see that multi-domain PINNs are more general and flexible than the existing PINN decomposition models such as XPINN and CPINN, and hence have more potentials. Having only

used XPINNs in Table 3, one might conclude decomposing this problem is inferior to a standard PINN. However, we have shown that CPINN outperformed XPINN by an order of magnitude and that adding the additional term I_{yy} improved the CPINN even further. Furthermore, naively adding all possible terms such as the final row, does not necessarily give the best results either. This leaves three options for multi-domain PINNs: manually tuning the interface conditions, running all possible permutations such as we have done here, or devise a method to learn the appropriate interfaces such as METALIC.

Model	L_2 Relative Error
PINN	1.05e-3 ± 4.38e-4
$I_{u_{avg}}$	4.28e-3 ± 2.63e-3
$I_{u_{avg}} + I_{rc}$	3.92e-3 ± 2.25e-3
$I_{u_{avg}} + I_c$	9.45e-4 ± 2.85e-4
$I_{u_{avg}} + I_{rc} + I_c$	9.77e-4 ± 3.45e-4
$I_{u_{avg}} + I_{rc} + I_{gr}$	4.57e-3 ± 3.18e-3
$I_{u_{avg}} + I_c + I_{yy}$	**5.26e-4 ± 1.97e-4**
$I_{u_{avg}} + I_{rc} + I_{gr} + I_c + I_{yy}$	9.34e-4 ± 3.18e-4

Table 4: Average L_2 relative error over 10 runs for different interface combinations. Note: $I_c = I_y$ for this problem.

Appendix C. Meta Learning Result Analysis

There are $2^9 = 512$ possible combinations of the interface conditions. For convenience, we use an integer to index each configuration (combination), index $= \sum_{i=0}^{n} 2^i \mathbf{c}[i]$ where $\mathbf{c}$ is a list of binaries, and $\mathbf{c}[i] = 1$ means i-th interface condition is turned on. We therefore can show how different sets of interface conditions are selected along with the equation parameters (see Figures 11, 14, 17, and 20).

C.1 Poisson Equation

For each PDE test case, we provide three analysis plots to better understand the METALIC results. For the Poisson problem, Figure 11 provides an overview of the interface configuration groupings as the equation parameter s varies. As opposed to Random-Single, the various METALIC methods predict interface configurations in groupings based on parameter s. This indicates that for these ranges, the PDE solution behaves similarly across the interfaces. It can also be seen that the configurations chosen between METALIC-Single and METALIC-Seq are different, indicating that the optimization is an important factor. This is logical since at the beginning of training, the PINN must first propagate information from the initial and boundary conditions inward to the entire domain. Therefore, interface conditions during this phase may in fact make learning more difficult in terms of the loss landscape as the network is trying to enforce continuity at a location which has no information but is simply a set of random predictions given the initialization of weights and bias of the network.

In Figure 12, we can see the number of times the interface conditions are selected over the 100 test cases. Random-Single serves as a baseline with each interface being chosen roughly half of the time. The two most noticeable trends are that the gradient-enhanced residual term is almost never chosen and the flux continuity which is equivalent to u_y for this case is always chosen by METALIC.

This is interesting as the gradient term in gPINNs was shown to be beneficial in PINN training but appears to be a poor chose on a set of interface points, possibly because with all the other terms, it simply make the loss landscape more complex and does not provide a significant accuracy benefit compared to the other more theoretically sound terms such as flux. This is a novel result as it proves the robustness of METALIC in being able to distinguish between valid and invalid terms, something that would take a user doing manual tuning of these terms much trail and error to determine. We also note that the METALIC choices align with our results in Section B.1 that the flux conditions from CPINN greatly outperforms the residual continuity conditions in XPINN for Poisson's equation. Flux continuity is a well studied conservation term rooted in traditional methods whereas residual continuity is a term devised with the convince of PINNs and automatic-differentiation(AD) in mind. We also note that when comparing the METALIC-Seq-UCB ADAM and L-BFGS choices, L-BFGS uses more terms on average than ADAM. This confirms our hypothesis from Figure 11 that more interface terms at the start of training may in-fact make it more difficult. This validates the result that not only is a sequential interface prediction more accurate, but also faster as it adds in terms as needed which would reduce computational cost. We also not that including the residual points in the overall set of collocation points is rarely chosen, likely due to the fact that the interface point set is an order of magnitude smaller than the collocation point set so assuming it is well sampling its contribution is negligible. All these insights further confirm the method is working well and is consistent with our intuition and the properties of the equation.

Finally, in Figure 13, we show the L^2 relative error as a function of s. This is a more detailed version of the error table in the manuscript which tells us how the problem difficulty changes over the parameterization of the problem. For this Poisson problem, it is quite consistent other than the lower bound around $s = 1$ in which the forcing term is very smooth and as we expect the problem is quite simple, as reflected by the lower errors there.
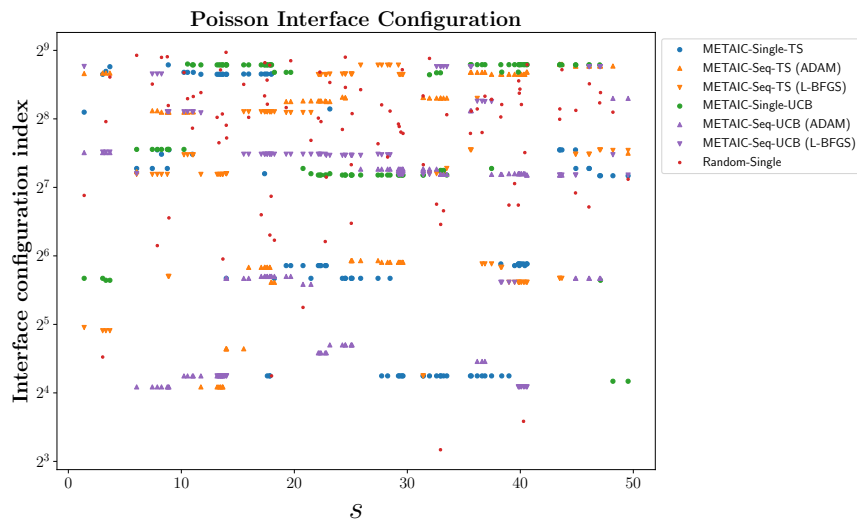

Figure 11: Scatter plot of interface configuration *vs.* the equation parameter s.
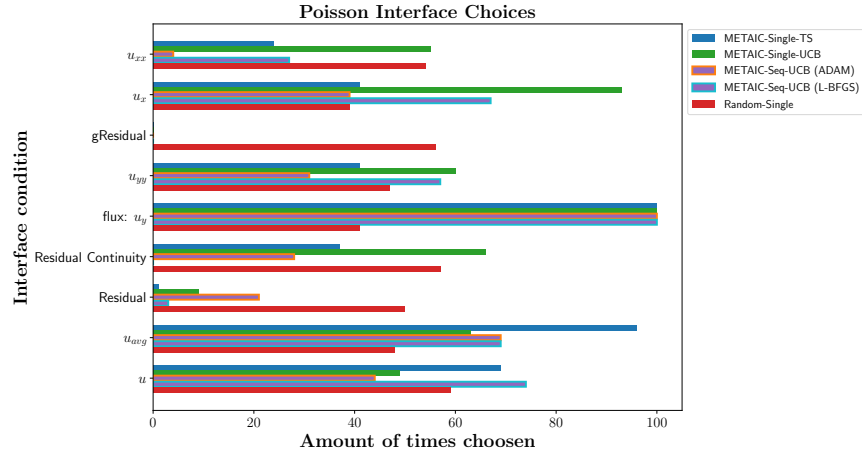
Figure 12: Horizontal bar plot of the quantity of interfaces chosen throughout testing over 100 randomly drawn equation parameters.
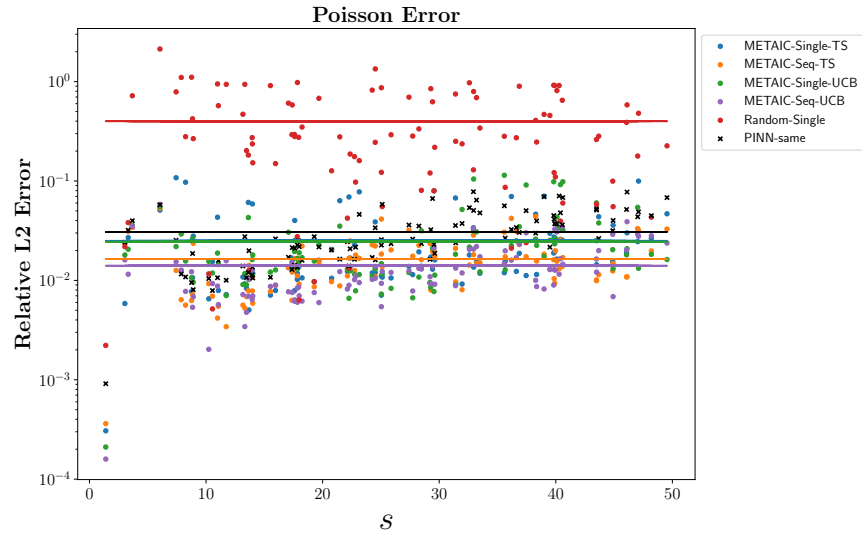

Figure 13: Scatter plot of the relative L_2 error *vs.* the equation parameter s.

C.2 Advection Equation

For the Advection problem, Figure 15 shows us that very few terms where needed in this case. So much so that the ADAM step of METALIC-Seq-UCB has only one term, $I_{u_{avg}}$, the weaker form of the solution continuity. We again point out the benefit of METALIC in being able to sub select few terms out of many while still resulting in the best accuracy as seen in Figures 14 & 16 which show that METALIC-Seq-UCB uses the fewest number of terms but has the best error. This emphasizes that more terms are not always better as the loss landscape in terms of optimization can become more complex. Another interesting feature is that the first derivative in space (u_x) is chosen more than the first derivative in time (u_t) despite the subdomain split being in time. This is opposite of the Poisson results in which the derivative normal to the interface (u_y), representing the flux, was chosen

in all cases. Both terms, u_t and u_x are part of the PDE with flux simply being u, but the tangential derivative u_x appears to be a much more meaningful term when it comes to propagating the wave through the interface. There are also no second order terms which was the case with Poisson.
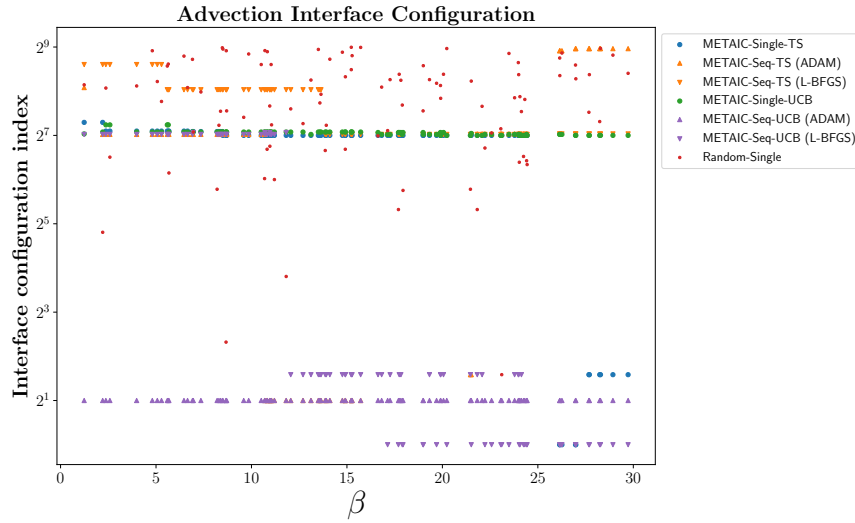

Figure 14: Scatter plot of interface configuration *vs.* the equation parameter β.
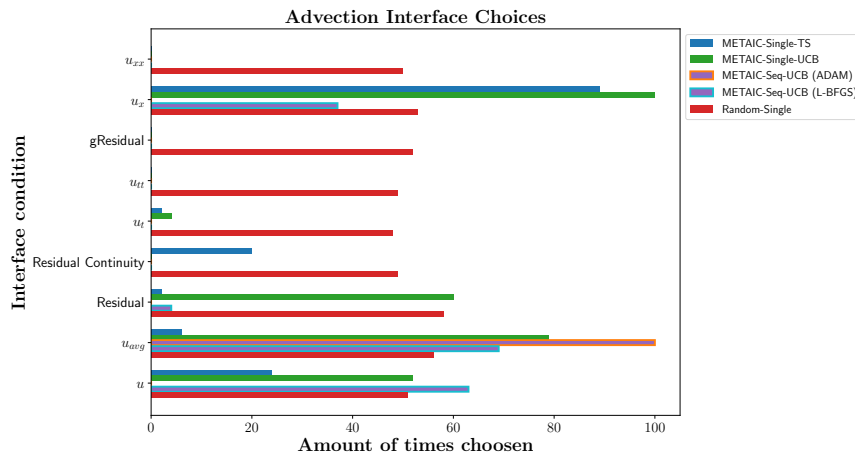
Figure 15: Horizontal bar plot of the quantity of interfaces chosen throughout testing over 100 randomly drawn equation parameters.
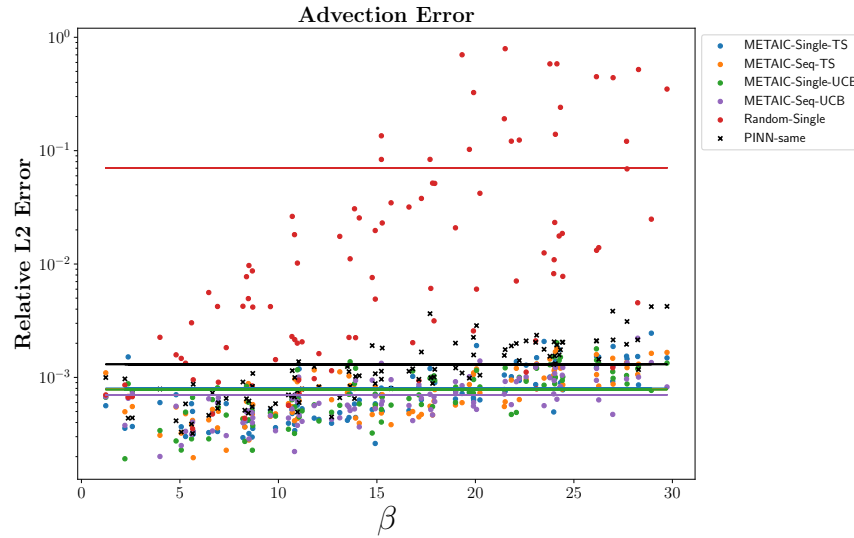
Figure 16: Scatter plot the relative L_2 error *vs.* the equation parameter β.

C.3 Reaction Equation

For the Reaction problem, it is interesting to note that whole this is an ODE, with no spatial derivatives, they were counter-intuitively chosen as interfaces. This emphasizes the fact that PINNs, and machine learning techniques in general, do not work the same as traditional methods as these terms are not necessary for well-posedness. Given this, Figure 19 shows that METALIC outperformed the PINN while using these conditions. This is an interesting line of investigation in the future as it shows counter-intuitive terms can provide a training benefit to PINNs even in contract to the previous Advection problem where almost no terms where chosen. It is not clear why in some cases only the most basic of terms are used while in others terms which do not make physical sense are chosen, but in both, the accuracy is quite good. This shows that METALIC learns something about training PINNs that is not evidently clear to the human user.
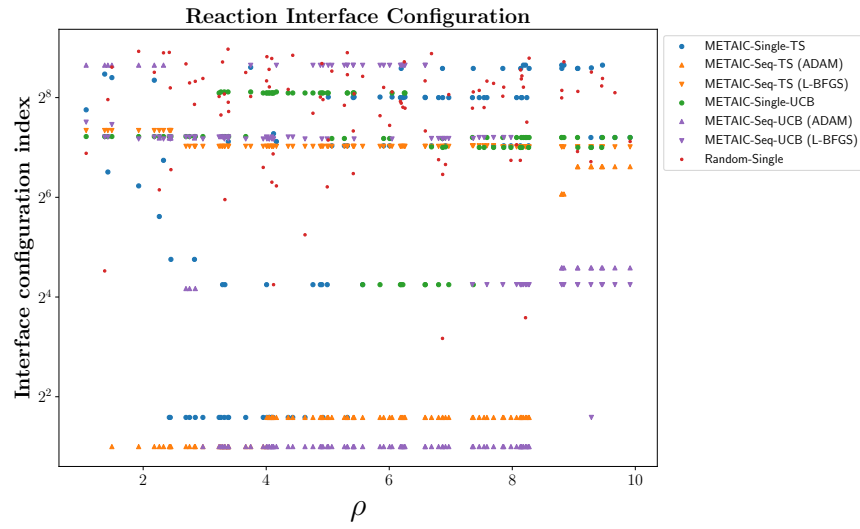
Figure 17: Scatter plot of interface configuration *vs.* the equation parameter ρ.
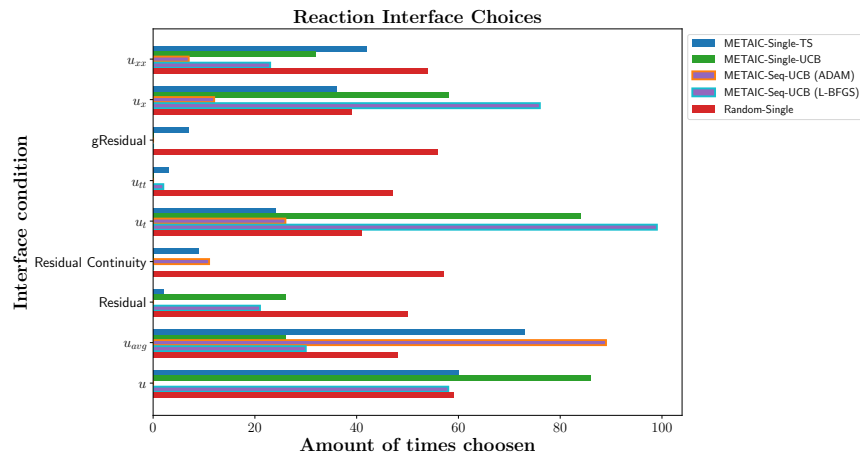

Figure 18: Horizontal bar plot of the quantity of interfaces chosen throughout testing over 100 randomly drawn equation parameters.
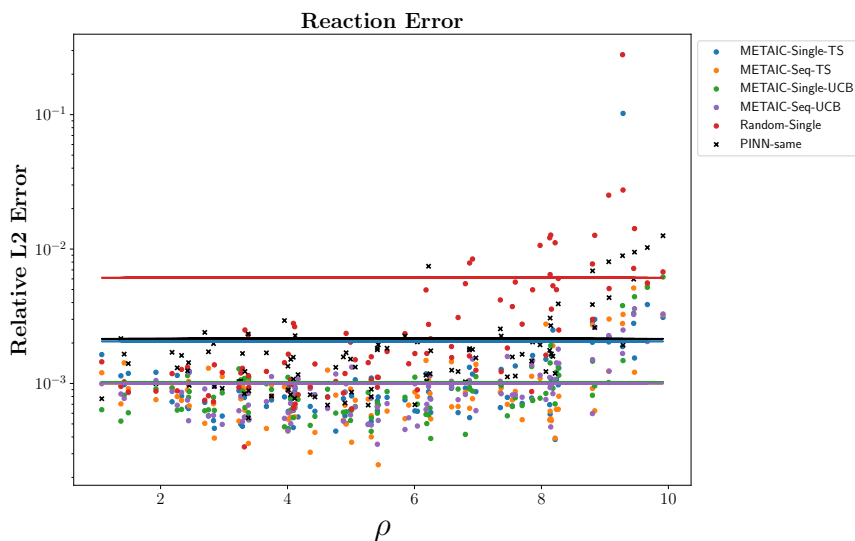
Figure 19: Scatter plot of the relative L_2 error *vs.* the equation parameter ρ.

C.4 Burger's Equation

For the Burger's problem, we see more of what one might expect from interface terms. Figure 21 shows that the flux term is predominately chosen, just as in Poisson's equation. Although here we see the flux is not equivalent to the first order derivative, enforcing the idea that it is in fact the flux providing the training benefit and not a coincidence of the first-order derivative and flux being the same for Poisson. We also see the largest improvement in error of METALIC over PINNs as seen in Figure 22. The trend is also consistent with our physical understanding, as viscosity (ν) increases the problem becomes more simple. This is because at lower viscosities a shock forms and creates a discontinuity in the solution which is difficult for PINNs to resolve. The decomposition of this problem is the most sound, in that we allow one network to handle the sharp discontinuity in the center, and another to handle the relatively simple solution around it. This allows for the network in the center to learn a higher frequency basis with which to approximate the discontinuity instead of also having to fit the lower frequencies around it which is delegated to the second network. Given this, it makes sense that a multi-domain PINN and METALIC greatly outperform PINNs here. It also emphasizes that in the less physically motivated decompositions for Poission, Advection, and Reaction, we still see improvement using multi-domain PINNs and METALIC.

25
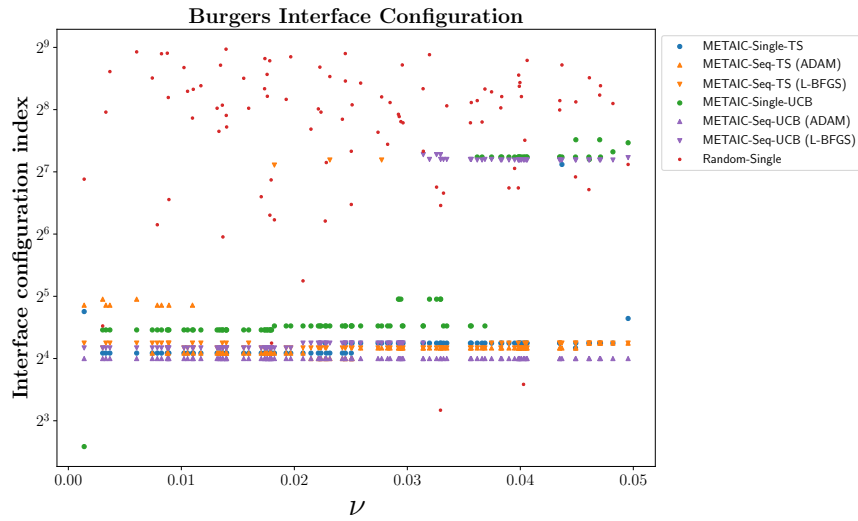
Figure 20: Scatter plot of interface configuration *vs.* the equation parameter ν.
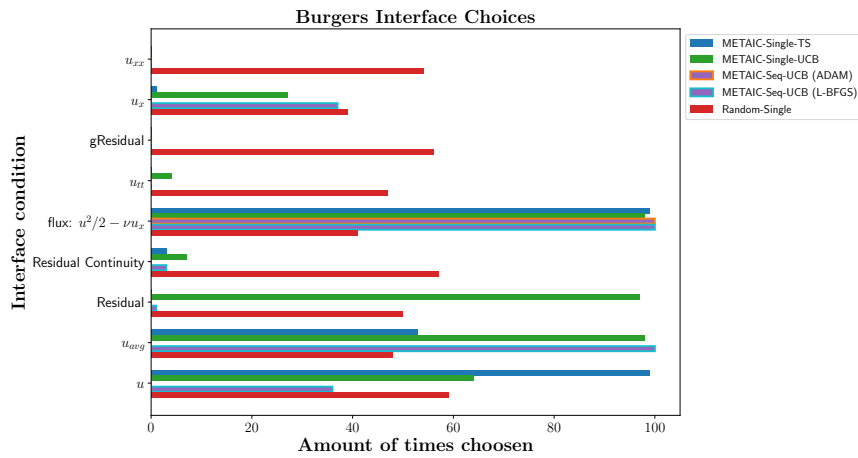

Figure 21: Horizontal bar plot of the quantity of interfaces chosen throughout testing over 100 randomly drawn equation parameters.
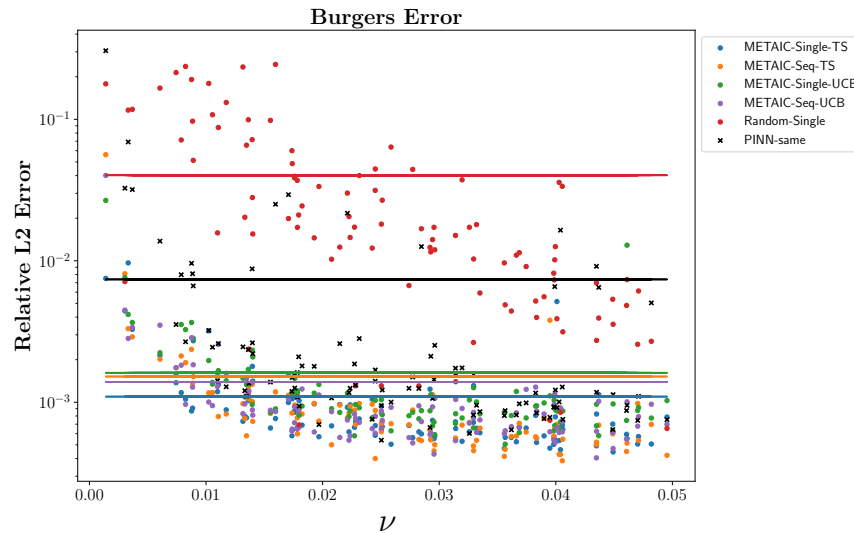
Figure 22: Scatter plot of the relative L_2 error *vs.* the equation parameter ν.

References

Kelsey Allen, Evan Shelhamer, Hanul Shin, and Joshua Tenenbaum. Infinite mixture prototypes for few-shot learning. In International Conference on Machine Learning, pages 232–241. PMLR, 2019.

Marcin Andrychowicz, Misha Denil, Sergio Gomez, Matthew W Hoffman, David Pfau, Tom Schaul, Brendan Shillingford, and Nando De Freitas. Learning to learn by gradient descent by gradient descent. arXiv preprint arXiv:1606.04474, 2016.

Peter Auer. Using confidence bounds for exploitation-exploration trade-offs. Journal of Machine Learning Research, 3(Nov):397–422, 2002.

Peter Auer, Nicolo Cesa-Bianchi, and Paul Fischer. Finite-time analysis of the multiarmed bandit problem. Machine learning, 47(2):235–256, 2002a.

Peter Auer, Nicolo Cesa-Bianchi, Yoav Freund, and Robert E Schapire. The nonstochastic multiarmed bandit problem. SIAM journal on computing, 32(1):48–77, 2002b.

Vashist Avadhanula, Riccardo Colini Baldeschi, Stefano Leonardi, Karthik Abinav Sankararaman, and Okke Schrijvers. Stochastic bandits for multi-platform budget optimization in online advertising. In Proceedings of the Web Conference 2021, pages 2805–2817, 2021.

Maryam Aziz, Emilie Kaufmann, and Marie-Karelle Riviere. On multi-armed bandit designs for dose-finding clinical trials. Journal of Machine Learning Research, 22(1-38):4, 2021.

Luca Bertinetto, Joao F Henriques, Philip HS Torr, and Andrea Vedaldi. Meta-learning with differentiable closed-form solvers. arXiv preprint arXiv:1805.08136, 2018.

Sébastien Bubeck, Nicolo Cesa-Bianchi, et al. Regret analysis of stochastic and nonstochastic multi-armed bandit problems. Foundations and Trends® in Machine Learning, 5(1):1–122, 2012.

Olivier Chapelle and Lihong Li. An empirical evaluation of thompson sampling. In Advances in neural information processing systems, pages 2249–2257, 2011.

Yuyao Chen, Lu Lu, George Em Karniadakis, and Luca Dal Negro. Physics-informed neural networks for inverse problems in nano-optics and metamaterials. Optics express, 28(8):11618–11633, 2020.

Tim De Ryck, Ameya D Jagtap, and Siddhartha Mishra. Error estimates for physics informed neural networks approximating the navier-stokes equations. arXiv preprint arXiv:2203.09346, 2022.

Yan Duan, John Schulman, Xi Chen, Peter L Bartlett, Ilya Sutskever, and Pieter Abbeel. Rl2: Fast reinforcement learning via slow reinforcement learning. arXiv preprint arXiv:1611.02779, 2016.

Zhiwei Fang and Justin Zhan. Deep physical informed neural networks for metamaterial design. IEEE Access, 8:24506–24513, 2019.

Chelsea Finn. Learning to learn with gradients. PhD thesis, UC Berkeley, 2018.

Chelsea Finn, Pieter Abbeel, and Sergey Levine. Model-agnostic meta-learning for fast adaptation of deep networks. In International Conference on Machine Learning, pages 1126–1135. PMLR, 2017.

Chelsea Finn, Kelvin Xu, and Sergey Levine. Probabilistic model-agnostic meta-learning. arXiv preprint arXiv:1806.02817, 2018.

Nicholas Geneva and Nicholas Zabaras. Modeling the dynamics of pde systems with physics-constrained deep auto-regressive networks. Journal of Computational Physics, 403:109056, 2020.

Erin Grant, Chelsea Finn, Sergey Levine, Trevor Darrell, and Thomas Griffiths. Recasting gradient-based meta-learning as hierarchical Bayes. In 6th International Conference on Learning Representations, ICLR 2018, 2018.

James Harrison, Apoorva Sharma, and Marco Pavone. Meta-learning priors for efficient online bayesian regression. In International Workshop on the Algorithmic Foundations of Robotics, pages 318–337. Springer, 2018.

Sepp Hochreiter, A Steven Younger, and Peter R Conwell. Learning to learn using gradient descent. In International Conference on Artificial Neural Networks, pages 87–94. Springer, 2001.

Zheyuan Hu, Ameya D Jagtap, George Em Karniadakis, and Kenji Kawaguchi. When do extended physics-informed neural networks (xpinns) improve generalization? arXiv preprint arXiv:2109.09444, 2021.

Ameya D Jagtap and George E Karniadakis. Extended physics-informed neural networks (xpinns): A generalized space-time domain decomposition based deep learning framework for nonlinear partial differential equations. In AAAI Spring Symposium: MLPS, 2021.

Ameya D Jagtap, Ehsan Kharazmi, and George Em Karniadakis. Conservative physics-informed neural networks on discrete domains for conservation laws: Applications to forward and inverse problems. Computer Methods in Applied Mechanics and Engineering, 365:113028, 2020.

Diederik P Kingma and Jimmy Ba. Adam: A method for stochastic optimization. arXiv preprint arXiv:1412.6980, 2014.

Georgios Kissas, Yibo Yang, Eileen Hwuang, Walter R Witschey, John A Detre, and Paris Perdikaris. Machine learning in cardiovascular flows modeling: Predicting arterial blood pressure from non-invasive 4d flow mri data using physics-informed neural networks. Computer Methods in Applied Mechanics and Engineering, 358:112623, 2020.

Gregory Koch, Richard Zemel, and Ruslan Salakhutdinov. Siamese neural networks for one-shot image recognition. In ICML deep learning workshop, volume 2. Lille, 2015.

Aditi Krishnapriyan, Amir Gholami, Shandian Zhe, Robert Kirby, and Michael W Mahoney. Characterizing possible failure modes in physics-informed neural networks. Advances in Neural Information Processing Systems, 34:26548–26560, 2021.

Tze Leung Lai, Herbert Robbins, et al. Asymptotically efficient adaptive allocation rules. Advances in applied mathematics, 6(1):4–22, 1985.

Michael Laskey, Jeff Mahler, Zoe McCarthy, Florian T. Pokorny, Sachin Patil, Jur van den Berg, Danica Kragic, Pieter Abbeel, and Ken Goldberg. Multi-armed bandit models for 2d grasp planning with uncertainty. In 2015 IEEE International Conference on Automation Science and Engineering (CASE), pages 572–579, 2015. doi: 10.1109/CoASE.2015.7294140.

Kwonjoon Lee, Subhransu Maji, Avinash Ravichandran, and Stefano Soatto. Meta-learning with differentiable convex optimization. In Proceedings of the IEEE/CVF Conference on Computer Vision and Pattern Recognition, pages 10657–10665, 2019.

Ke Li and Jitendra Malik. Learning to optimize. arXiv preprint arXiv:1606.01885, 2016.

Shuai Li, Alexandros Karatzoglou, and Claudio Gentile. Collaborative filtering bandits. In Proceedings of the 39th International ACM SIGIR conference on Research and Development in Information Retrieval, pages 539–548, 2016.

Zhenguo Li, Fengwei Zhou, Fei Chen, and Hang Li. Meta-sgd: Learning to learn quickly for few-shot learning. arXiv preprint arXiv:1707.09835, 2017.

Dehao Liu and Yan Wang. Multi-fidelity physics-constrained neural network and its application in materials modeling. Journal of Mechanical Design, 141(12), 2019.

Hao Liu, Richard Socher, and Caiming Xiong. Taming maml: Efficient unbiased meta-reinforcement learning. In International Conference on Machine Learning, pages 4061–4071. PMLR, 2019.

Aditya Mahajan and Demosthenis Teneketzis. Multi-armed bandit problems. In Foundations and applications of sensor management, pages 121–151. Springer, 2008.

Nikhil Mishra, Mostafa Rohaninejad, Xi Chen, and Pieter Abbeel. A simple neural attentive meta-learner. arXiv preprint arXiv:1707.03141, 2017.

Tsendsuren Munkhdalai and Hong Yu. Meta networks. In International Conference on Machine Learning, pages 2554–2563. PMLR, 2017.

Devang K Naik and Richard J Mammone. Meta-neural networks that learn by learning. In [Proceedings 1992] IJCNN International Joint Conference on Neural Networks, volume 1, pages 437–442. IEEE, 1992.

Boris N Oreshkin, Pau Rodriguez, and Alexandre Lacoste. Tadam: Task dependent adaptive metric for improved few-shot learning. arXiv preprint arXiv:1805.10123, 2018.

Michael Penwarden, Shandian Zhe, Akil Narayan, and Robert M Kirby. Physics-informed neural networks (pinns) for parameterized pdes: A metalearning approach. arXiv preprint arXiv:2110.13361, 2021.

Maziar Raissi, Paris Perdikaris, and George E Karniadakis. Physics-informed neural networks: A deep learning framework for solving forward and inverse problems involving nonlinear partial differential equations. Journal of Computational Physics, 378:686–707, 2019a.

Maziar Raissi, Zhicheng Wang, Michael S Triantafyllou, and George Em Karniadakis. Deep learning of vortex-induced vibrations. Journal of Fluid Mechanics, 861:119–137, 2019b.

Maziar Raissi, Alireza Yazdani, and George Em Karniadakis. Hidden fluid mechanics: Learning velocity and pressure fields from flow visualizations. Science, 367(6481):1026–1030, 2020.

Sachin Ravi and Hugo Larochelle. Optimization as a model for few-shot learning. In In International Conference on Learning Representations (ICLR), 2017.

Francisco Sahli Costabal, Yibo Yang, Paris Perdikaris, Daniel E Hurtado, and Ellen Kuhl. Physics-informed neural networks for cardiac activation mapping. Frontiers in Physics, 8:42, 2020.

Adam Santoro, Sergey Bartunov, Matthew Botvinick, Daan Wierstra, and Timothy Lillicrap. Meta-learning with memory-augmented neural networks. In International conference on machine learning, pages 1842–1850. PMLR, 2016.

Jürgen Schmidhuber. Evolutionary principles in self-referential learning, or on learning how to learn: the meta-meta-... hook. PhD thesis, Technische Universität München, 1987.

Khemraj Shukla, Ameya D Jagtap, and George Em Karniadakis. Parallel physics-informed neural networks via domain decomposition. Journal of Computational Physics, 447:110683, 2021.

Justin Sirignano and Konstantinos Spiliopoulos. Dgm: A deep learning algorithm for solving partial differential equations. Journal of computational physics, 375:1339–1364, 2018.

Aleksandrs Slivkins et al. Introduction to multi-armed bandits. Foundations and Trends® in Machine Learning, 12(1-2):1–286, 2019.

Jake Snell, Kevin Swersky, and Richard Zemel. Prototypical networks for few-shot learning. Advances in neural information processing systems, 30, 2017.

Xingyou Song, Wenbo Gao, Yuxiang Yang, Krzysztof Choromanski, Aldo Pacchiano, and Yunhao Tang. Es-maml: Simple hessian-free meta learning. In ICLR, 2020.

Niranjan Srinivas, Andreas Krause, Sham Kakade, and Matthias Seeger. Gaussian process optimization in the bandit setting: no regret and experimental design. In Proceedings of the 27th International Conference on International Conference on Machine Learning, pages 1015–1022, 2010.

Luning Sun, Han Gao, Shaowu Pan, and Jian-Xun Wang. Surrogate modeling for fluid flows based on physics-constrained deep learning without simulation data. Computer Methods in Applied Mechanics and Engineering, 361:112732, 2020.

Richard S Sutton and Andrew G Barto. Reinforcement learning: An introduction. MIT press, 2018.

William R Thompson. On the likelihood that one unknown probability exceeds another in view of the evidence of two samples. Biometrika, 25(3/4):285–294, 1933.

Sebastian Thrun and Lorien Pratt. Learning to learn. Springer Science & Business Media, 2012.

Oriol Vinyals, Charles Blundell, Timothy Lillicrap, Koray Kavukcuoglu, and Daan Wierstra. Matching networks for one shot learning. arXiv preprint arXiv:1606.04080, 2016.

Jane X Wang, Zeb Kurth-Nelson, Dhruva Tirumala, Hubert Soyer, Joel Z Leibo, Remi Munos, Charles Blundell, Dharshan Kumaran, and Matt Botvinick. Learning to reinforcement learn. arXiv preprint arXiv:1611.05763, 2016.

Sifan Wang, Yujun Teng, and Paris Perdikaris. Understanding and mitigating gradient flow pathologies in physics-informed neural networks. SIAM Journal on Scientific Computing, 43(5):A3055–A3081, 2021.

Sifan Wang, Xinling Yu, and Paris Perdikaris. When and why pinns fail to train: A neural tangent kernel perspective. Journal of Computational Physics, 449:110768, 2022.

Jaesik Yoon, Taesup Kim, Ousmane Dia, Sungwoong Kim, Yoshua Bengio, and Sungjin Ahn. Bayesian model-agnostic meta-learning. In Proceedings of the 32nd International Conference on Neural Information Processing Systems, pages 7343–7353, 2018.

Jeremy Yu, Lu Lu, Xuhui Meng, and George Em Karniadakis. Gradient-enhanced physics-informed neural networks for forward and inverse pde problems. Computer Methods in Applied Mechanics and Engineering, 393:114823, 2022.

Fengwei Zhou, Bin Wu, and Zhenguo Li. Deep meta-learning: Learning to learn in the concept space. arXiv preprint arXiv:1802.03596, 2018.

Yinhao Zhu, Nicholas Zabaras, Phaedon-Stelios Koutsourelakis, and Paris Perdikaris. Physics-constrained deep learning for high-dimensional surrogate modeling and uncertainty quantification without labeled data. Journal of Computational Physics, 394:56–81, 2019.

Luisa Zintgraf, Kyriacos Shiarli, Vitaly Kurin, Katja Hofmann, and Shimon Whiteson. Fast context adaptation via meta-learning. In International Conference on Machine Learning, pages 7693–7702. PMLR, 2019.